Interference of Acoustic Signals Due to Internal Waves in Shallow Water

*Young-Nam Na, *Mun-Sub Jurng, *Taebo Shim

Abstract

To investigate the characteristics of internal waves (IWs) and their effects on acoustic wave propagation, a series of sea experiment were performed in the east coast of Donghae city, Korea in 1997 and 1998 where the water depth varies between 130 and 140 m. Thermistor strings were deployed to measure water temperatures simultaneously at 9 depths. CW source signals with the frequencies of 250, 670 and 1000 Hz were received by an array of 15 hydrophones. Through the Wavelet transform analysis, the IWs are characterized as having typical periods of 2-17 min and duration of 1-2 hours. The IWs exist in a group of periods rather than in one period. Underwater acoustic signals also show obvious energy peaks in the periods of less than 12 min. Consistency in the periods of the two physical processes implies that acoustic waves react to the IWs through some mechanisms like mode interference and travel time fluctuation. Based on the thermistor string data, mode arriving structures are analyzed. As thermocline depth varies with time, it may cause travel time difference as much as 4-10 ms between mode 1 and 2 over 10 km range. This travel time difference causes interference among modes and thus fluctuation from range-independent stratified ocean structure. In real situations, however, there exist additional spatial variation of IWs. Model simulations with all modes and simple IWs show clear responses of acoustic signals to the IWs, i.e., fluctuations of amplitude and phase.

Ⅰ. Introduction

Whenever a sufficient vertical density gradient exists in ocean, internal waves (IWs, from now on) restored by buoyancy can occur. Because they owe their existence to the restoring force due to the density gradient and the Coriolis force, the frequency spectra of IWs are bounded by the inertial frequency at the low end and by the buoyancy frequency at the high end. Typical IWs are characterized by temperature and velocity fluctuations with periods from tens of second to several hours, and with scales from 100 m to 10 km in the horizontal, and 1 to 100 m in the vertical. It is important mechanism for mixing and energy transport in both the shallow and the deep ocean [1].

In shallow water, IWs appear in a deterministic nature and are characterized by being propagated as solitary waves or solitons [2]. The soliton is a wave-packet-like propagating disturbance that keeps its shape because of the opposing effects of dispersion (tending to spread the packet) and nonlinear effects (tending to steepen and confine the packet). The internal solitons with large amplitude (Figure 1) have been observed in numerous coastal area and lakes [2], although not all observed solitary perturbations are solitons [3]. In shallow water, deterministic groups of IWs with well-defined wavelengths are usually observed during summer when they are trapped in a strong and shallow seasonal thermocline. Solitons have been found to be highly

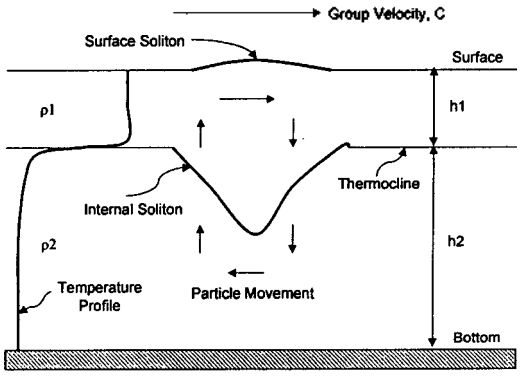

Figure 1. Schematic picture showing solitary internal wave in the thermocline layer.

* Agency for Defense Development
Manuscript Received:March 2, 1999

correlated with the tides and to propagate shoreward. They seem to be generated by the interaction of a tidally driven flow with sills, continental shelf edges, or other major variations in underwater topography [2].

Acoustically, temperature fluctuation causes changes in sound speed, which in turn lead to the fluctuations of travel time of pulse signal. Internal wave-induced ocean variability in temporal and spatial domain has been found to be a very significant source of sound scattering and has received considerable attention in recent years [4-6]. Many techniques based on the ray or mode theory are available to study acoustic variability associated with IWs. In deep water, the ray theory has proven to be a useful tool [5]. In shallow water, Essen et al. [7] conducted an analysis of phase variability based on modal perturbations. Zhou et al. [2] studied the resonant scattering of acoustic energy by internal-wave solitons using the mode coupling theory. Recently, Lynch et al. [8] have used both modal and ray based perturbation techniques to compare predicted travel time variance results to measured variances in the Barents Sea Polar Front (BSPF) experiment.

The East Sea of Korea is believed to have IWs because of strong thermocline during summer. Calculations with historical CTD data show that IWs may exist with periods from a few minutes to 20 hours, where the maximum period varies with latitude [9]. Lim [10] and Lee [11] analyzed the role of internal tides and relations with temperature variations in the East Sea. However, there are few studies on the IWs of shorter periods. This study aims at analyzing the spectrum characteristics of the IWs of less than one hour period and at investigating their effects on acoustic wave propagation.

A series of oceanographic experiments were conducted in 1997 and 1998 in the water of 130-140 m deep. Thermistor strings were deployed to investigate characteristics of the IWs. In order to examine acoustic wave responses to the IWs, an acoustic experiment was also performed at the same area of oceanographic survey in 1998. The acoustic experiment used a sound source and an array of hydrophones, each being moored for an hour and separated about 5 km horizontally. It was originally designed to conduct the oceanographic experiment to estimate the IWs effects on underwater acoustic signals but the two experiments were not made simultaneously. Hence, this paper does not attempt to compare directly the two data sets, IWs and acoustic waves, but just delivers spectra patterns. Also, travel time variance is estimated based on the thermistor string data and experimental conditions. Finally, the fluctuations of acoustic pressure fields due to simple IWs are demonstrated using the model, RAM [12], which is based on the parabolic equation technique.

Ⅱ. Characteristics of Internal Waves and Acoustic Signals

A. Sea Experiment

In order to investigate the characteristics of IWs, sea experiments were conducted in the East Sea off Donghae city in 1997 and 1998. Figure 2 shows the locations where equipment was installed during the experiments. In 1998, two thermistor strings, each having 9 temperature sensors every 10m, were deployed to estimate the direction and the speed of the IWs. The water depth varies from 130 m to 140m. The thermistor strings (TR7-1, 2) were designed to gather data every 10sec. The oceanographic experiments were performed at the same location TR7-2 in 1997 and TR7-1, 2 in 1998. There was actually no wind (wave-height was below 0.5 m) so that the weather allowed very nice condition to perform the experiments.

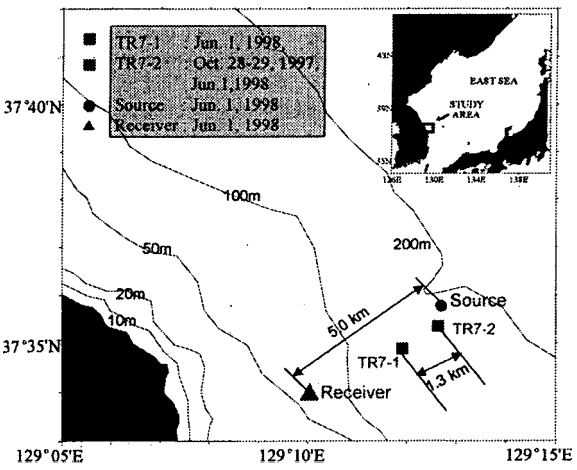

Figure 2. Station map of oceanographic and acoustic experiments.

An acoustic experiment was conducted to examine underwater acoustic signal responses to the IWs. It was designed to conduct the oceanographic experiment at the same area and time, but major oceanographic equipment had to be retrieved before the acoustic experiment due to the bad weather. The two sea trials have time difference of two hours.

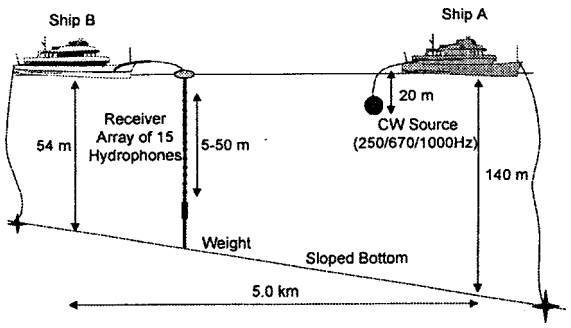

Figure 3. Schematic picture showing acoustic experiment of Jun. 1, 1998. The two survey ships, being around 5 km away each other, were moored to deploy a source and an array of hydrophones for an hour.

Figure 3 shows the source and the receiver configuration. The two survey ships were moored to deploy a sound source and an array of hydrophones for an hour. The source was located at 20 m depth and made to project continuous wave (CW) signals of 250, 670, and 1000 Hz, the water depth being 140 m. The location is very near to the one (TR7-2) for the IWs measurement. The vertical line array, which covers 45 m with 15 hydrophones, was deployed at depth between 5-50 m. Since the water depth is 54 m, the array covers more than 80 % of the water column. The first 11 hydrophones are arranged at every 2.5 m (coverage is 2.5x10 = 25 m) and others at every 5 m (coverage is 5x4 = 20 m).

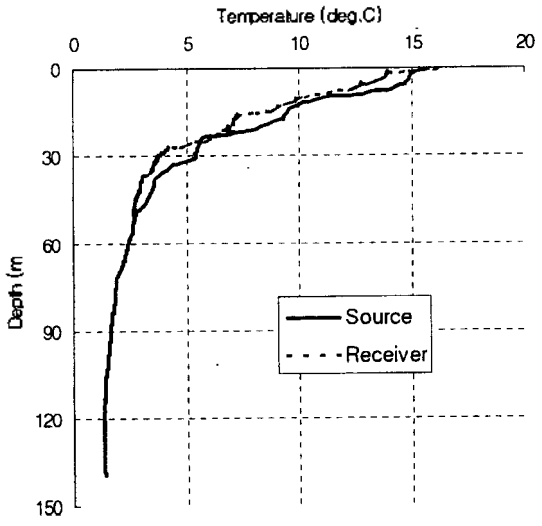

Figure 4. Vertical temperature profiles at the source and the receiver stations.

Temperature profiles at two stations (Figure 4) represent step-wise thermocline from the surface to 30 m deep. Although the two profiles show similar structures, the one at the source gives higher temperatures at the same depths.

B. Spectrum Characteristics of Internal Waves

Through the time series of the thermistor string data, one can see that they show time-varying patterns rather than consistent patterns. In this situation, the conventional spectrum analysis like the Fourier transform may fail to extract major characteristics of the IWs. This study employs the Wavelet transform [13] to examine the IWs features. The Wavelet transform analysis is capable of revealing aspects of data that other signal analysis misses, aspects like trends, breakdown points, discontinuities in higher derivatives, and self-similarity [14].

Figure 5 gives the coefficients of the Wavelet transform with the thermistor string data in 1997. The x-axis represents scale, which increases up to the maximum frequency (i. e., sampling frequency 10 sec), and the y-axis represents time along the signal. The numbers in the x-axis show scale indices and can be changed into frequency through the formula $2^{(j/12+1)}/10240$, where j indicates scale index. For example, index 60 leads to $2^{(60/12+1)}/10240 = 6.25\times10^{-3}$ Hz (or 2.7 min). The grade in each x-y plot represents the magnitudes of the Wavelet coefficients. A set of 1024 data, where the sampling interval is 10 sec, stands for about 170 min.

The Wavelet transform with the data of October 28 (46 m) shows clear features of the IWs, which can be specified by the periods of 2.4-5.7 min at the time step of 100-140. The results with the data of October 29 (42, 51 m) also give obvious IWs characteristics in time and period (Fig. 5b,c). The first 1024 data at 42 m depth show that there are two IWs events at the time steps of 0-60 and 80-130, the former having a little shorter periods than the latter. At 51 m depth, however, the former event is not clear while the latter still represents IWs traces with the periods of 2.0-5.3 min.

The thermistor string data in 1998 also show the IWs characteristics well in time-scale domain (Figure 6). The Wavelet coefficients are based on the first 2048 data (about 341 min) at the station TR7-1 (onshore) and TR7-2 (offshore). At the depth of 8 m, the IWs exist at the time step of 50-200, their periods being decreased with time from 11.3 to 2.0 min. At 18 m depth, the IWs exist at the wider range of periods, their maximum period being extended to 16.9 min. The other two figures (Figure 6c,d) show that the duration time of the IWs somewhat decreases, resulting in sharper peaks. However, the

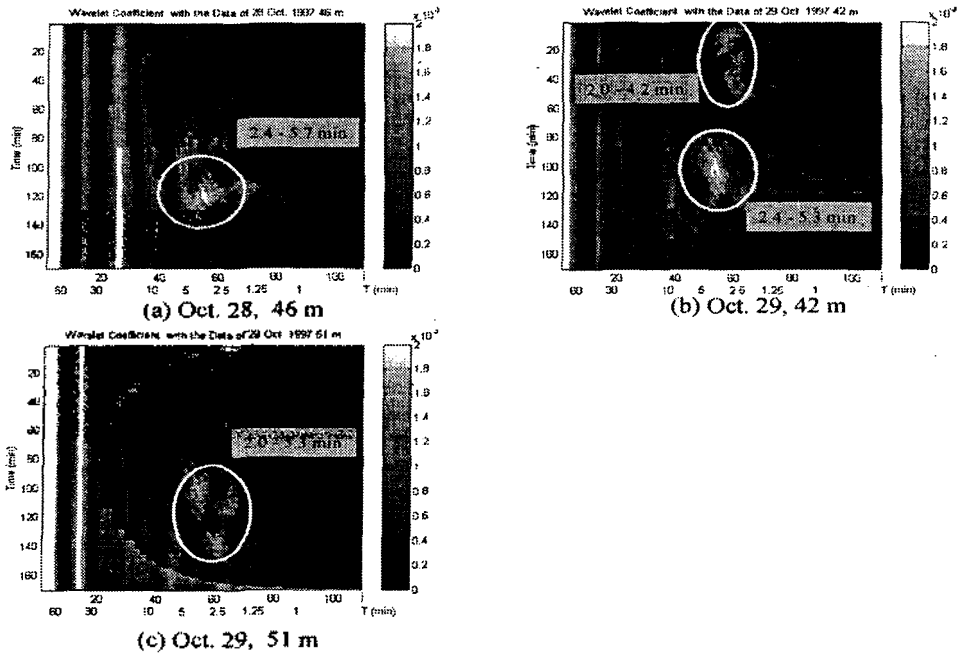

Figure 5. Wavelet transform results of thermistor string data (1997, TR-2) in time-scale domain. (a) Oct. 28, 55.3 m, (b) Oct. 29, 41.7 m, (c) Oct. 29, 51.2 m.

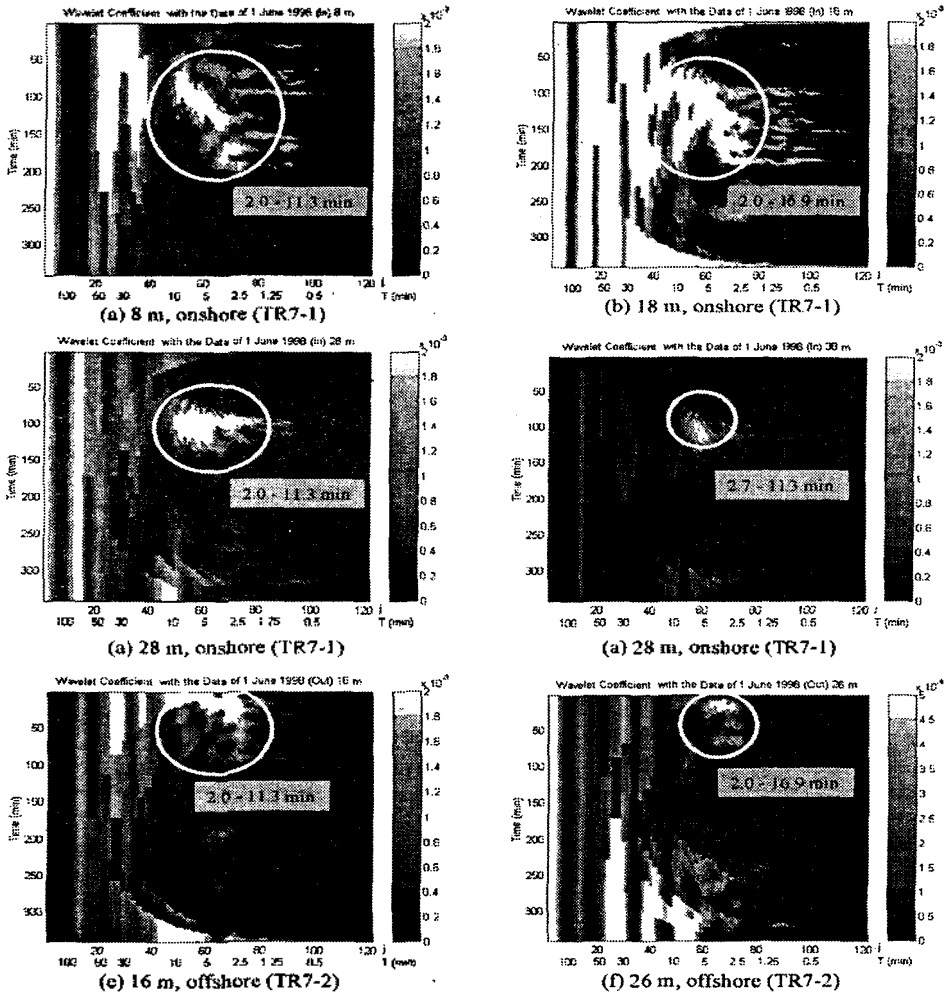

Figure 6. Wavelet transform results of thermistor string data (June 1, 1998) in time-scale domain. (a) 8 m, onshore (TR7-1), (b) 18 m, onshore (TR7-1), (c) 28 m, onshore (TR7-1), (d) 38 m, onshore (TR7-1), (e) 16 m, offshore (TR7-2), (f) 26 m, offshore (TR7-2).

periods still exist in 2.0-11.3 min. Interesting thing is that the IWs exist in a group of periods rather than in one period. In Figure 5 and 6, some large coefficients can be seen in the longer period (specially at 18 m depth on June 1, Figure 6b). This phenomenon occurs when there exists consistent temperature increase which might be caused by consistent transport of warm water mass [15].

Throughout the Wavelet transform analysis, one can see that the IWs have the periods of 2-17 min and continue for 1-2 hours. According to Kim et al. [9], who estimated the possible periods of IWs in the East Sea, the minimum period is an order of 2 min. The minimum period can be estimated by the relation $T_{min} = 60/N_{max}$, where N_{max} is the maximum buoyancy frequency. Assuming the latitude of 36°N, the maximum period (inertial period) is $T_{max} = 12/\sin 36^{\circ} = 20.4$ hours. Hence, the periods in this study are consistent with the predicted results. Concerning the spatial characteristics of IWs such as direction and wavelength, future studies and experiments should be followed.

C. Time Variation of Received Signals

The acoustic signals received by 15 hydrophones are recorded on tapes and digitized every 1 sec. Figure 7 shows amplitude distribution in sensor number (depth) and time. The amplitude in dB scale has been calibrated by hydrophone sensitivity and amplifier gain. The source frequencies of 250, 670 and 1000 Hz correspond to the source level of 165 dB, and the propagation loss (in dB) between source-receiver can be computed by subtracting received signal level (dB) from 165 dB.

At the frequency of 250 Hz, one can see very large signal level fluctuations in time particularly at sensors # 5 and 13. The large signal levels continue for more than 500 sec with fluctuation ranges up to 25 dB. This time variation is caused typically by the fluctuation of ocean environments through which acoustic waves propagate. Ocean fluctuations have very wide range of scales in space and time. Among the ocean fluctuations, this study focuses on the IWs effects on acoustic wave propagation. The large signal levels may be due to constructive interference caused by the IWs. The way how the IWs cause acoustic waves to result in interference is described in later section.

At the frequency of 670 Hz, there exist no noticeably large levels as in previous case but still exist in small scales. At the time step of 2500-3300 sec, small signal

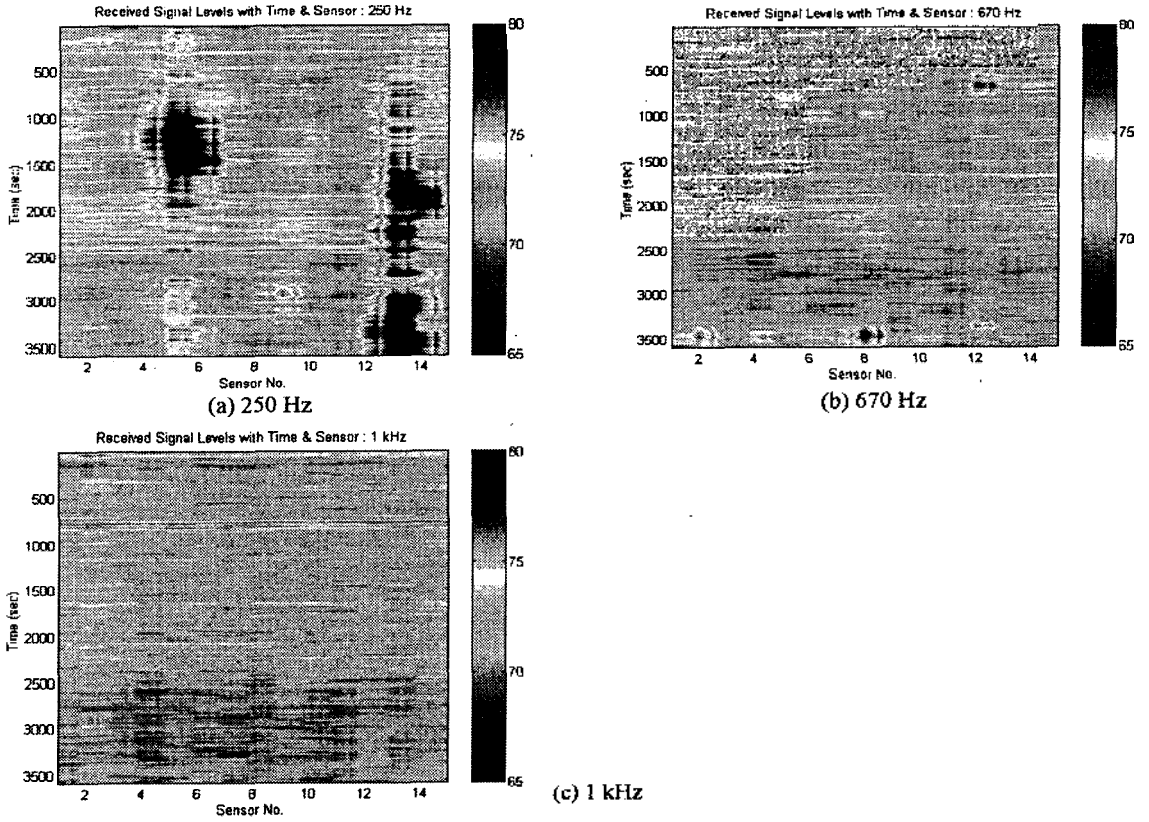

Figure 7. Received signal levels (dB) with sensor number and time. (a) 250 Hz, (b) 670 Hz, (c) 1 kHz.

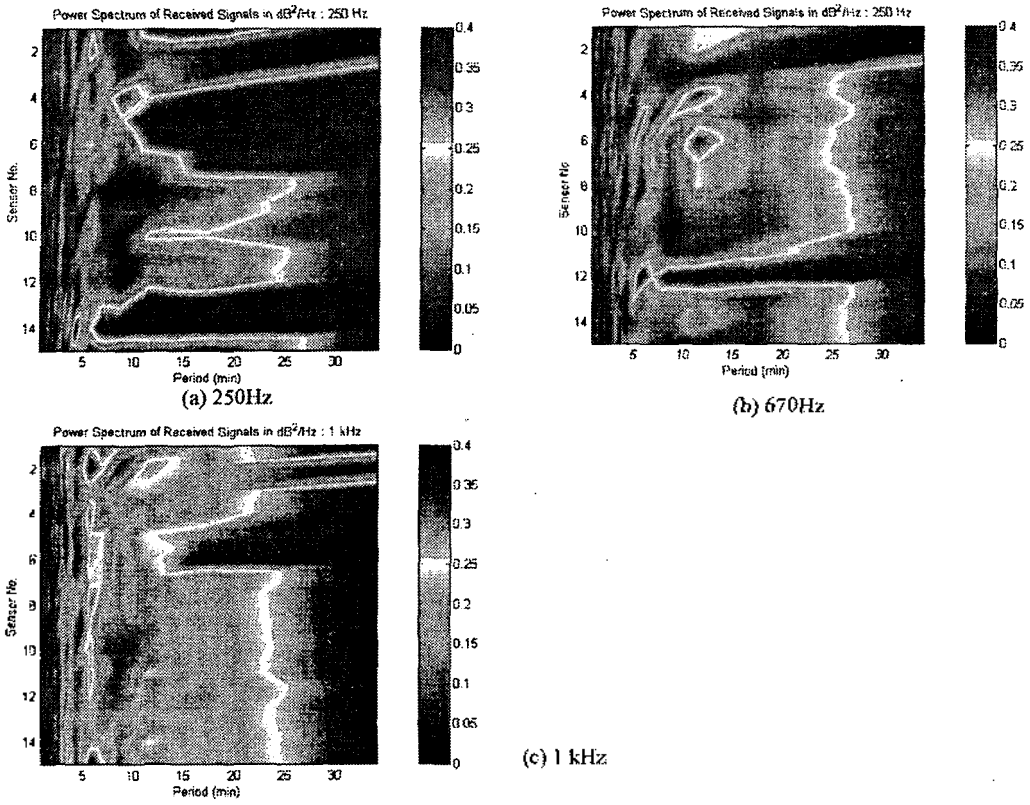

Figure 8. Spectra of underwater acoustic signals (1998) in sensor-period domain. (a) 250 Hz, (b) 670 Hz, (c) 1 kHz.

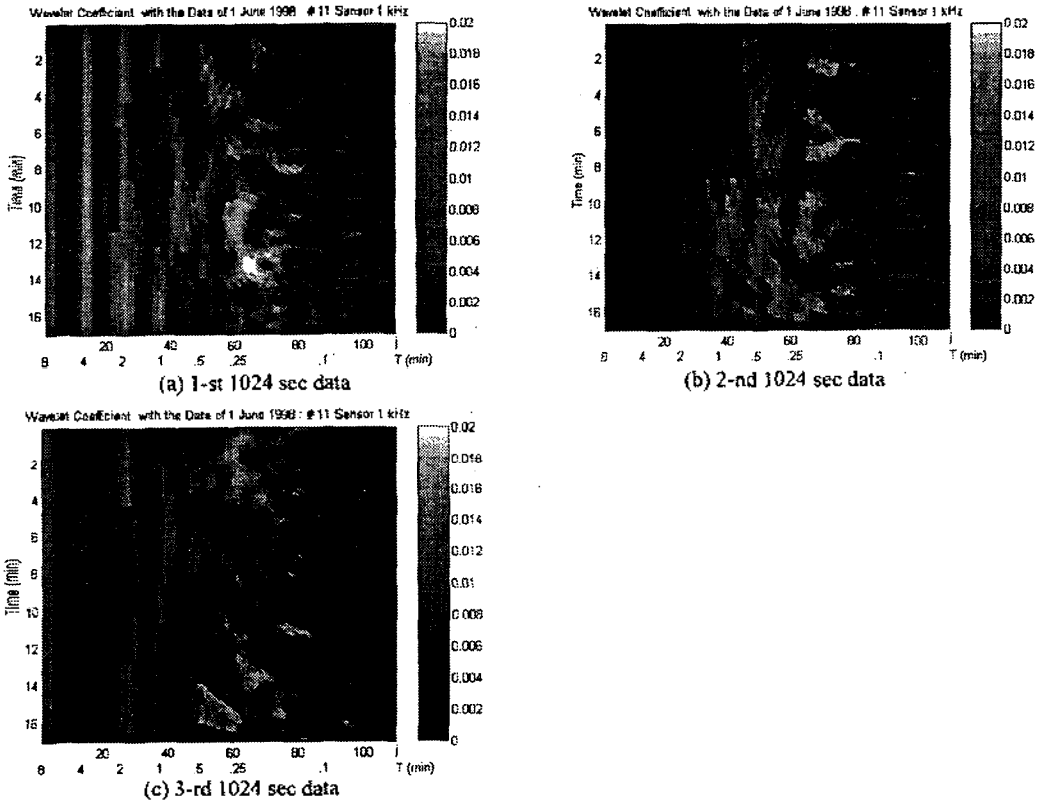

Figure 9. Wavelet transform results of underwater acoustic signals (1 kHz) received by sensor # 11 at depth 30m. (a) 1-st 1024 sec data (b) 2-nd 1024 sec data, (c) 3-rd 1024 sec data.

levels (below 73 dB) can be seen throughout all sensors. This phenomenon is thought to be due to destructive interference of acoustic waves [2]. These smaller levels can also be seen at the same time step at 1 kHz. In addition, at the time step of 500-1000 sec, a zone of higher signal levels (about 3 dB greater than the neighbors) develops for 100 sec throughout the entire sensors.

D. Spectrum Characteristics of Acoustic Signals

Power spectrum levels (in dB^2/Hz) are obtained through the Fourier transform with the whole data. Figure 8 shows spectrum distributions in period-time domain at three frequencies. At the frequency of 250 Hz, the energy in longer periods (more than 25 min) is large except at sensor # 2, where small energy exists throughout the periods. At sensors # 11 and 12 (depth 30.5 and 35.5 m), the energy is large until the period of 10 min. One can see some peaks in the periods of 5-10 min. At the frequency of 670 Hz, relatively small energy exists at sensor # 2, but at others large energy exists in the periods of longer than 25 min. Relatively large energy is located in the periods of 5-12 min particularly at sensors # 4, 6, and 12. At 1 kHz, the trend of large energy in longer periods is also maintained. Very great peaks are extracted in the periods of 12 and 6 min, those in 6 min existing over all sensors. Some peaks in shorter periods (less than 4 min) are shown in the three distributions.

To examine the patterns of shorter periods, the Wavelet transform is again employed. Figure 9 gives the Wavelet coefficients with successive three 1024 data sets at 1 kHz and at sensor # 11 (30 m). The scale index 60 corresponds to $2^{(60/12+1)}/1024 = 6.25\times10^{-2}$ Hz (0.27 min). The signals are sampled every 1 sec so that 1024 data covers about 17 min. Power spectra with the whole data (Fig. 8) show only period information but the Wavelet coefficients give the information on scale (period or frequency) and time. With the 1-st 1024 data set, one can see that the energy in the periods of 4.3 min (j =12) and 2.1 min (j =24) is dominant over the time. Other peaks correspond to the periods of 0.2-0.9 min. With the 2-nd and 3-rd data sets, many peaks exist within these small periods. All these peaks in 0.2-0.9 min are believed to contribute to the peaks in small periods in Fig. 8.

Acoustic signal spectra reveal that narrow-band energy (or peak) exists in periods less than 12 min while broad-band energy is dominant in longer periods. The peaks sometimes occur over whole sensors as in 4, 6 min of 1 kHz signal. It is interesting that the two physical processes, fluctuations of IWs and acoustic waves, show same range of periods, 2-17 min. This consistency in periods between the two processes may be verified through simultaneous measurement of the IWs and acoustic waves.

Ⅲ. Mode Arriving Structure

To estimate travel time difference of acoustic waves due to the IWs variation, this study employs the simplified formula based on the ray-mode theory. The normal mode theory is widely accepted in calculating the sound pressure fields. The mode eigenfunction and wavenumber are two important components analyzing propagating fluctuation. The ray-mode theory can give very intuitive idea of acoustic responses to thermocline. Zhang et al. [16] presented the simplified formula of the horizontal wavenumbers and the group velocities from the ray-mode theory. Here, we briefly describe the formula.

The grazing angle θ_m of the eigenray of the m-th mode satisfies the following equation.

$$k_0 \cos\theta_m = \mu_m, \tag{1}$$

where $k_0 = \omega / c_0$, and μ_m is the eigenvalue which can be estimated from the equation of eigenvalue as shown

$$2\sqrt{k_0^2 - \mu_m^2}\,h = 2(m-1)\pi + \frac{\pi}{2} + \varphi_b(\mu_m), \tag{2}$$

where h is the thickness of water below the thermocline as shown in Fig. 10, and (φ_b is the phase shift at the bottom. Thus the group velocity can be expressed as following :

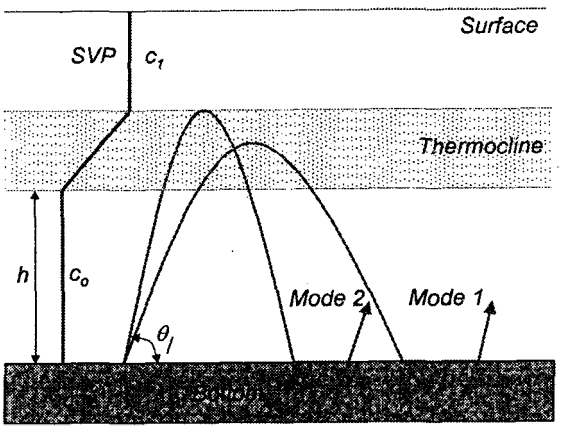

Figure 10. Schematic picture showing the mode propagation through thermocline.

$$v_m = c_0 \cos\theta_m = c_0 \sqrt{1 - \left[\frac{2(m-1)\pi + \pi/2 + \varphi_b(\mu_m)}{4} \frac{c_0}{fh}\right]^2}. \tag{3}$$

It is clear that the thermocline depth is critical to group velocities. For the several modes, where the grazing angles of the corresponding energy are small, the asymptotical formula for group velocities can be used and $\varphi_b(\mu_m)$ can be fixed to $\pi/2$ for simplicity. The time delay between mode 1 and m at range r is then expressed as :

$$\tau_{1m} = r\left[v_{nl}^{-1} - v_m^{-1}\right] \approx \frac{1}{32} \frac{rc_0}{f^2 h^2}\left[(2m-1)^2 - 1\right], \tag{4}$$

and the influence of the thermocline depth variation on time delay variation is derived by taking derivative of τ with respect to h, which is

$$\left|\frac{\partial \tau_{1m}}{\partial h}\right| \approx \frac{1}{16} \frac{rc_0}{f^2 h^2}\left[(2m-1)^2 - 1\right]. \tag{5}$$

Here, the thermocline depth h, which is a function of time, is obtained by finding the depth of temperature 6°C from the thermistor string data. The temperature 6°C is assumed to be the lower limit of thermocline depth.

It can be seen from Eq. (4) that the group velocities are closely dependent on the thermocline depth. The group delay varies inverse proportionally to the square of the depth of the thermocline and the square of signal frequency. So, the smaller h is, the greater the group delay variation will be. From Figure 4, one may obtain the depth h below the thermocline as 110 m. When the temperature is 6°C, the simple formula [17] leads to sound velocity of about 1476 m/s at depth 100 m. Assuming r = 10 km and f = 250 Hz, the travel time difference between the first two modes and its depth derivative are computed as 4.9 ms and 0.1 ms/m, respectively.

Figure 11 shows the travel time difference between mode 1 and 2, which is calculated using Eq. (4). Here, the source-receiver range is assumed to be 10 km and the frequency 250 Hz. The thermocline depth h is obtained via interpolating the isothermal depth of 6°C from the four temperature data sets whose locations are marked in Figure 2. From the temperature profile at the source (Figure 4), one can see that the depth corresponding to 6°C is roughly lower limit of thermocline. Since the sampling interval is 10 sec, the time sequence 1800 yields 18000 sec (or 5 hours). The first two curves (Figure 11a) shows that they vary within some range of variation, 9-12 ms. Between the last two curves (Figure 11b), however, there exist large difference reaching almost 3.0 ms at the time

Table 1. Mean and variance of thermocline depth (h) and travel time difference ((12) between mode 1 and 2, where r = 10 km and f = 250 Hz.

	TR7-2 (28 Oct. 1997) Mean	Var.	TR7-2 (29 Oct. 1997) Mean	Var.	TR7-1 (1 June 1998) Mean	Var.	TR7-2 (1 June 1998) Mean	Var.
Thermocline Depth, h	74.88	1.94	75.66	7.67	103.52	33.32	115.70	22.72
Travel Time Difference, τ_{12}	10.54	0.15	10.36	0.56	5.56	0.34	4.43	0.12

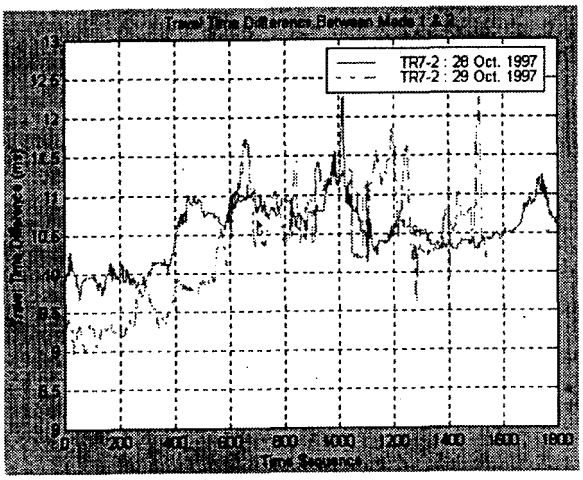

(a) 28-29 Oct., 1997

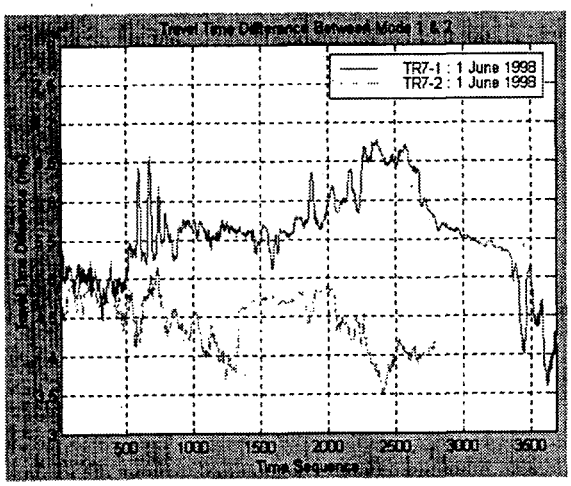

(b) 1 June., 1998

Figure 11. Travel time difference with time sequence, where the difference is between mode 1 and 2. The range r is assumed to be 10 km and the frequency 250 Hz. (a) Oct. 28-29, 1997, (b) Jun. 1, 1998.

sequence of 2400. Noticing the fact that the first two data have same position with one day jump but the second two data have same time with 1.3 km away, one can see that travel time difference (or thermocline depth) varies more with space than time.

Table 1 summarizes statistical characteristics of thermocline depth and travel time difference for the four data sets. The variance of thermocline depth reaches up to 33 m at TR7-1 (June 1, 1998). Meanwhile, that of travel time difference between mode 1 and 2 varies from 0.12 to 0.56 ms over 10 km range. This travel time difference causes interference among modes and thus fluctuations from (range-independent) stratified ocean structure. This simple calculation here considers only time variation effect of thermocline (i.e., IWs variation at one point). In real situations, however, there exist additional spatial variation of the IWs. The following section demonstrates the spatial effects of the IWs on acoustic wave propagation through model simulations.

Ⅳ. Model Simulation

A. Model Input

To simulate the spatial variation of pressure fields due to the IWs, simple IWs are generated as following formula :

$$z(d) = d - A(d)\sin(2\pi r/\lambda_i), \tag{6}$$

where $z(d)$ = depth variation, d = depth of the IWs, r = horizontal range, λ_i = wavelength. The amplitude $A(d)$ is defined as $10\cos(|20-d|(\pi/20)$, where d exists between 10 and 30 m depth. The IWs consist of five waves of each wavelength 200 m so that they cover horizontal range of 1 km, starting at the range of 1 km. Figure 12 shows the input sound speed structure with the IWs characteristics.

As for geoacoustic data, the parameters of sand-silt-clay are considered. The typical values are sound velocity c_b = 1500 m/s, density ρ_b= 1500 kg/m^3, and attenuation α_b = 0.8 dB/λ [18]. The water depth is 140 m and the sound source is located at 20 m, the center depth of the IWs.

B. Model

The model RAM (range-dependent acoustic model) is based on the parabolic equation (PE) technique. The PE method is very effective for solving range-dependent ocean problems. RAM was developed using the split step Pade' solution [19], which allows large range steps, and is the most effective PE algorithm that has been developed. We just describe final results of pressure fields in range-independent case.

In cylindrical coordinates, the pressure field in range increment Δr can be obtained as following :

$$p(r+\Delta r, z) = \exp(ik_0\Delta r)\left(1+\sum_{j=1}^{n}\frac{\gamma_{j,n}X}{1+\beta_{j,n}X}\right)p(r,z), \tag{7}$$

where the operator

$$X = k_0^{-2}\left(\rho\frac{\partial}{\partial z}\frac{1}{\rho}\frac{\partial}{\partial z}+k^2-k_0^2\right), k_0 = \omega/c_0, \tag{8}$$

and c_0 is a representative phase speed. The complex coefficients $\gamma_{j,n}, \beta_{j,n}$ are defined by placing accuracy and stability constants on the rational function.

The self starter for a point source is employed in the form

$$p(r_0, z) = \frac{\exp(ik_0 r_0(1+X)^{1/2})}{k_0^{1/2}(1+X)^{1/4}}\delta(z-z_0). \tag{9}$$

To avoid encountering singular intermediate solutions, RAM solves Eq. (9) with the following approach :

$$(1-X)^2 q(z) = k_o^{-1/2}\delta(z-z_o), \tag{10}$$

$$p(r_o, z) = (1+X)^{7/4}\exp(ik_o r_o(1+X)^{1/2})q(z). \tag{11}$$

The intermediate function q has two continuous derivatives. The depth operator X is discretized using Galerkin' s method as described in [20]. In RAM version 1.0, the factor $(1+X)^2$ was used to smooth the delta function. In later version, however, it was replaced by the factor $(1-X)^2$. This change directs more improved stability. The factor $(1+X)^2$ is nearly singular for some problems involving deep water and/or weak sediment attenuation coefficients.

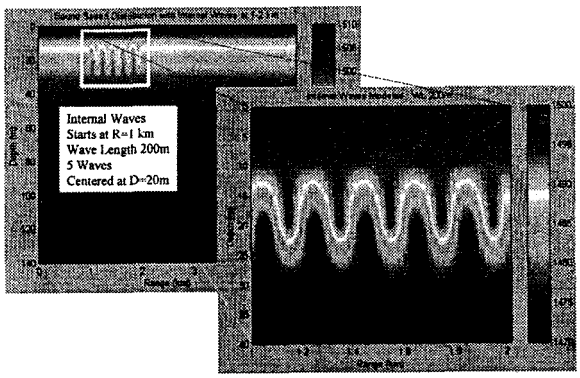

Figure 12. IWs characteristics for the model simulation. The IWs exist between 1 and 2 km (5 waves) range with 200 m in wavelength.

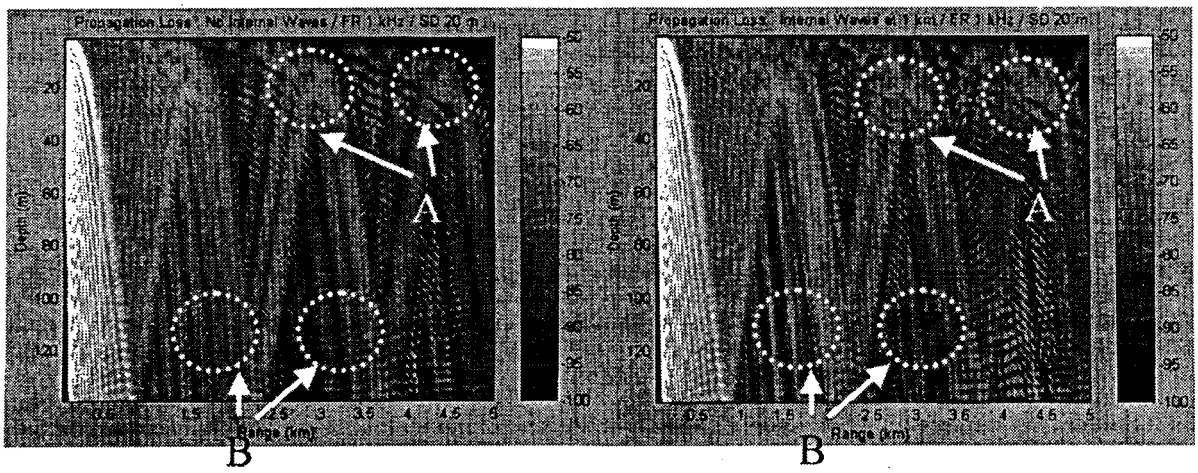

(a) No IWs (b) IWs

Figure 13. Propagation loss variation when the source exists within the IWs (SD 20m). (a) no IWs, (b) IWs.

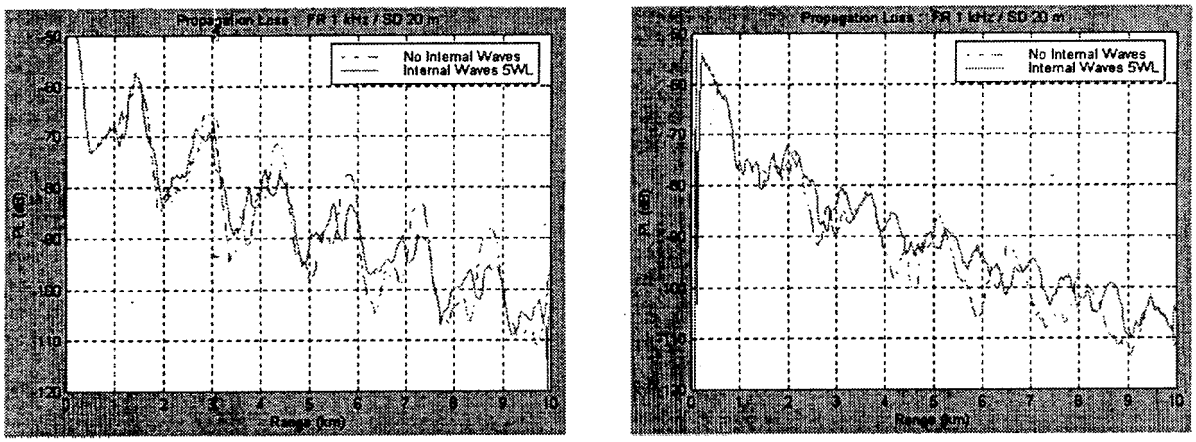

(a) RD 20m (b) RD 140m

Figure 14. Propagation loss at some receiver depths when the source exists within the IWs (SD 20 m). (a) RD 20m, (b) RD 140m.

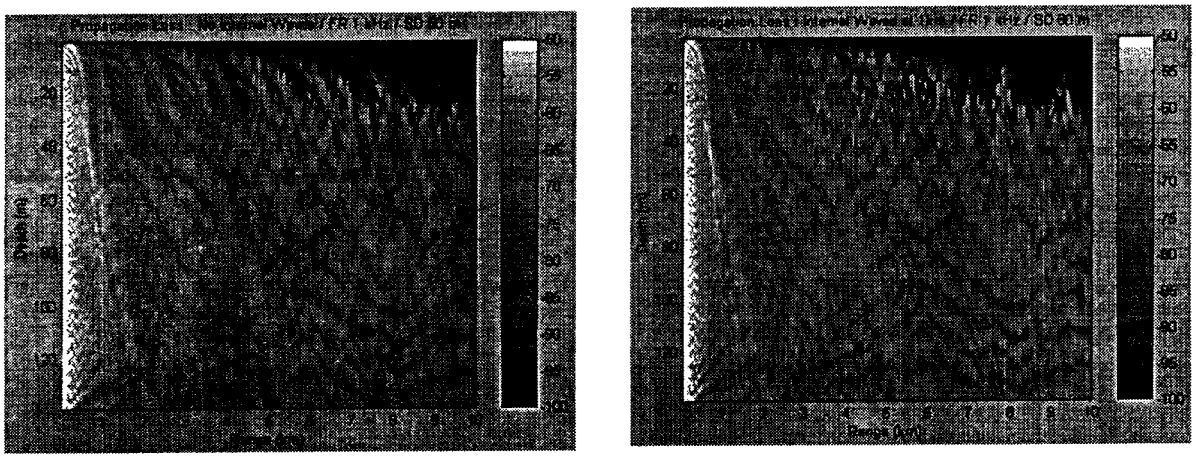

(a) No IWs (b) IWs

Figure 15. Propagation loss variation when the source exists below the IWs (SD 80 m). no IWs, (b) IWs.

For range-dependent problems, it is necessary to specify a condition at the vertical interfaces between regions. That is, accurate solutions may be obtained by conserving energy flux, and thus by modifying operator X.

C. Results

Figure 13 shows two distributions of propagation loss when the IWs exist and when there are no IWs. The sound source is located at 20 m depth and its frequency is 1 kHz. It can be seen that the two results give exactly same distribution until the range of 1 km, where the IWs start, but give some difference thereafter. That is, the regions marked as 'A', which represents convergence zones of acoustic energy, appear to be distorted when the IWs exist. At near the bottom, acoustic energy bundles marked as 'B' show significant difference between the two cases. Examining the propagation loss difference at some receiver depths (Fig. 14), one can see the IWs effects on acoustic wave propagation. At the receiver depth of 20 m with no IWs, very regular surface convergence zones develop every 1.4 km. With the IWs, however, these convergence zones tend to be distorted and the degree increases as the range increases. At 140 m depth, the bottom, one can find no prominent convergence zones. Instead, irregular fluctuations exist with range. The amplitudes seem to be out of phase between the two curves, resulting in more than 10 dB difference at some ranges. When the source is located within the IWs, acoustic waves proved to undergo additional interference, which causes difference in magnitudes and phases of their pressure fields.

When the source depth changes into 80 m, below the thermocline, the distributions of propagation loss (Fig. 15) show significant difference compared with the case of 20 m depth. The most noticeable point is that the acoustic energy seems to be trapped below the thermocline. As a result, no surface convergence zones are formed. This is comprehensible because most of acoustic waves refract down in the thermocline layer and thus few of them 'feel' the IWs during propagation.

The model simulation includes all of the possible modes while the travel time estimation in the previous section is attempted for the first two modes. Moreover, the estimation is made for the case when the source exists on the bottom. If the travel time variance is estimated including all the modes, it may give larger value. (Even larger value is expected when the sound source exists within the IWs!) The travel time fluctuations of acoustic wave due to the IWs may cause interference between modes.

V. Conclusions

Through the Wavelet transform analysis, the IWs are characterized as having typical periods of 2-17 min and duration of 1-2 hours. The IWs exist in a group of periods rather than in one period. Underwater acoustic signals also show obvious energy peaks in the periods of less than 12 min. The consistency in the periods of the two physical processes implies that acoustic waves react to the IWs through some mechanisms like mode interference and travel time fluctuation.

Based on the thermistor string data, mode arriving structures are analyzed. As thermocline depth varies with time at one point, it may cause travel time difference as much as 4-10 ms between mode 1 and 2 over 10 km range. This travel time difference causes interference among modes. At one time, the IWs have variations in space that lead to acoustic signal fluctuations. Model simulation with all modes and simple IWs show clear responses of acoustic signals to the IWs, fluctuations of amplitude and phase.

Further studies should be followed to investigate spatial features such as propagating directions and wavelengths. To have more productive results on the IWs effects on acoustic signal propagation, joint experiments of oceanography and acoustics are highly required.

Acknowledgements

The authors would like to express thanks to Prof. J. Y. Na in Hanyang University and other anonymous reviewers for their careful review. They also wish to appreciate to Drs. W. H. Cho and S. M. Choi in ADD for their kind suggestions which made possible to improve this paper. The thermistor data sets were gathered from the sea experiments conducted under the project *Study on Characteristics of Internal Waves in the East Sea* in UARC (Underwater Acoustics Research Center).

References

1. Garret and W. Munk, "Internal waves in the ocean," *Ann. Rev. Fluid Mech.* Vol. 11, pp. 339-69, 1979.
2. J. X. Zhou and X. Z. Zhang, P. H. Rogers, "Resonant

interaction of sound wave with internal solitons in the coastal zone," *J. Acoust. Soc. Am.*, Vol. 90, Pt. 1, pp. 2042-2054, 1991.

3. L. A. Otrovsky and Y. U. Stepanyants, "Do internal solitons exist in the ocean?", *Rev. Geophysics*, Vol. 27, pp. 293-310, 1989.
4. Y. Desaubies, Statistical aspects of sound propagation in the ocean, in Adaptive Methods in Underwater Acoustics, ed. H. Urban, The Netherlands: Dordrecht, Reidel, 1985.
5. S. M. Flatté, R. Dashen, W. H. Munk, K. M. Watson, and F. Zachariasen, Sound Transmission Through a Fluctuating Ocean, Cambridge : Cambridge University Press, 1979
6. B. J. Uscinski, C. Macaskill, and T. E. Ewart, "Intensity fluctuations, Pt. I: theory, Pt. II: comparison with the Cobb experiment," *J. Acoust. Soc. Am.*, Vol. 74, pp. 1474-1499, 1979.
7. H. H. Essen, F. Schiemer, and S. Sirkes, "Acoustic remote sensing of internal waves in shallow water," Int. *J. Remote Sens.*, Vol. 4, pp. 33-47, 1983.
8. J. F. Lynch, J. Guoliang, R. Pawlowicz, D. Ray, C. S. Chiu, J. Miller, R. H. Bourke, R. Parson, A. Pluedemann, and R. Muench, "Acoustic travel time perturbations due to the shallow water internal waves and internal tides in the Barents sea polar front: Theory and experiment," *J. Acoust. Soc. Am.*, Vol. 99, pp. 803-821, 1996.
9. K. Kim, J. Y. Na, S. C. Park and W. J. Seong. Annual Report : Unerwater Acoustics Modeling Laboratory. Underwater Acoustics Research Center Rep., 1999.
10. H. J. Lie, C. W. Shin and Y. H. Seung, "Internal Tidal Oscillation of Temperature off Jukbyun on the East Coast of Korea," *J. Kor. Soc. Ocean.*, Vol. 27(3): 228-236, 1992.
11. K. S. Lim., "Internal Tides in an Axially Symmetric Basin," *J. Kor. Soc. Ocean.*, Vol. 26(2), pp. 133-143, 1991.
12. M. D. Collins, User' s Guide for RAM Version 1.0 and 1.0p, Document of Naval Research Laboratory, pp. 1-13, 1997.
13. I. Daubechies, "The Wavelet Transform, Time-Frequency Localization and Signal Analysis," *Trans. Infrom Theory*, Vol. 36(5), pp. 961-1005, 1990.
14. M. Misiti, Y. Misiti, G. Oppenheim and J. M. Poggi, Wavelet Toolbox User' s Guide, THE MATH WORKS Inc., pp. 1-34, 1996.
15. Y. N. Na, T. B. Shim, H. R. Kim, and K. Kim, "Spectrum Characteristics of Internal Waves and Underwater Acoustic Signals in the East Sea of Korea," Submitted to *J. Kor. Soc. Ocean.*, May 1999.
16. R. H.Zhang, J. Q. Ziao and M. Gong, "Analysis of individual modes in shallow water," *Chinese Journal of Acoustics*, Vol. 3(3), pp. 238-249, 1984.
17. C. C. Leroy, "Development of Simple Equations for Accurate and More Realistic Calculation of the Speed of Sound in Sea Water," *J. Acoust. Soc. Am.*, Vol. 46, p. 216, 1969.
18. J. F. Miller and S. N. Wolf, Modal Acoustic Transmission Loss (MOATAL) : A Transmission Loss Computer Program Using a Normal-Mode Model of the Acoustic Field in the Ocean, Naval Reseach Lab., Rep. No. 8429, pp. 1-126, 1980.
19. M. D. Collins, "Generalization of the split-step Padá solution," *J. Acoust. Soc. Am.* Vol. 96, pp. 382-385, 1993.
20. M. D. Collins and E. K. Westwood, "A higher-order energy-conserving parabolic equation for range-dependent ocean depth, sound-speed, and density," *J Acoust. Soc. Am.*, Vol. 89, pp. 1068-1075, 1991.

▲ Young-Nam Na
Senior Research Scientist, Agency for Defense Development (Vol. 17, No. 2E, 1998)

▲ Mun-Sub Jurng
Senior Research Scientist, Agency for Defense Development (Vol. 17, No. 2E, 1998)

▲ Taebo Shim
Chief Research Scientist, Agency for Defense Development (Vol. 17, No. 2E, 1998)